

DeepVoting: An Explainable Framework for Semantic Part Detection under Partial Occlusion

Zhishuai Zhang¹, Cihang Xie¹, Jianyu Wang², Lingxi Xie¹, Alan L. Yuille¹

¹ Department of Computer Science, The Johns Hopkins University, Baltimore, MD 21218 USA

² Baidu Research (USA), Sunnyvale, CA 94089 USA

{zhishuai.zhang, cihangxie306, wjyouch, 198808xc, alan.l.yuille}@gmail.com

Abstract

In this paper, we study the task of detecting semantic parts of an object. This is very important in computer vision, as it provides the possibility to parse an object as human do, and helps us better understand object detection algorithms. Also, detecting semantic parts is very challenging especially when the parts are partially or fully occluded. In this scenario, the popular proposal-based methods like Faster-RCNN often produce unsatisfactory results, because both the proposal extraction and classification stages may be confused by the irrelevant occluders.

To this end, we propose a novel detection framework, named DeepVoting, which accumulates local visual cues, called visual concepts, to locate the semantic parts. Our approach involves adding two layers after the intermediate outputs of a deep neural network. The first layer is used to extract visual concept responses, and the second layer performs a voting mechanism to capture the spatial relationship between visual concepts and semantic parts. The benefit is that each semantic part is supported by multiple visual concepts. Even if some of the supporting visual concepts are missing due to occlusion, we can still infer the presence of the target semantic part using the remaining ones. To avoid generating an exponentially large training set to cover all occlusion cases, we train our model without seeing occlusion and transfer the learned knowledge to deal with occlusions. This setting favors learning the models which are naturally robust and adaptive to occlusions instead of over-fitting the occlusion patterns in the training data. In experiments, DeepVoting shows significantly better performance on semantic part detection in occlusion scenarios, compared with Faster-RCNN, with one order of magnitude fewer parameters and $2.5 \times$ testing speed. In addition, DeepVoting is explainable as the detection result can be diagnosed via looking up the voted visual concepts.

Introduction

Object detection is a fundamental computer vision task which attracts a lot of research attentions. Recently, object detection is dominated by a family of proposal-based approaches (Girshick et al. 2014; Girshick 2015; Ren et al. 2015; Lin et al. 2017; He et al. 2017), which generates a number of object proposals on the image, and applies a classifier to distinguish between them. On the other hand, semantic part detection, despite its importance, has been much less studied (Wang et al. 2015a). A *semantic part* is a fraction of an object which can be verbally described, such as a

wheel of a *car* or a *wing* of an *airplane*. Detecting semantic parts is a human ability, which enables us to recognize or parse an object especially when it is partially occluded.

In this paper, we investigate semantic part detection especially when these parts are partially or fully occluded. This is a very challenging task, and the proposal-based detection methods may not produce satisfying performance, as both the proposal extraction and classification stages can be largely distracted and confused: when a part is occluded by an irrelevant object, the original proposal for this region may be missing, and, even if there is one, the classification may go wrong since the occluder can be of arbitrary appearance. We will verify this in our experiments.

This motivates us to develop an alternative framework, which accumulates mid-level visual cues for inference. Following (Wang et al. 2015a), we consider *visual concepts*, which are obtained from the intermediate states of a deep neural network, as the mid-level visual cues. We build connections between these visual concepts and the semantic parts, which take both appearance and spatial relationship into consideration. Our approach is named **DeepVoting** as we explicitly use the visual concepts to *vote* for semantic parts, *e.g.*, detecting a *car side bottom* region may suggest that there are *car wheels* nearby. This strategy works well in dealing with occlusion, since each semantic part is supported by a number of visual concepts. *Even if some of them are missing due to occlusion, the remaining ones especially those voting from a long distance away can still reveal the presence of the target semantic part.*

A highlight of our work is that we train our model *only* on occlusion-free image data. The motivation is that humans are able to learn from non-occluded objects, memorize the spatial relationship between visual cues and semantic parts, and transfer these knowledge to deal with occlusion. We also desire computer vision algorithms to have such ability. This strategy also avoids generating exponentially many training samples (the number, appearance and position of occluders can be almost arbitrary). At the testing stage, we investigate two scenarios, *i.e.*, whether occlusion is present or not. In the latter case, we randomly place some irrelevant *occluders* onto each image, and compute the occlusion level by the fraction of occluded pixels on the object. DeepVoting significantly outperforms Faster-RCNN (Ren et al. 2015), the state-of-the-art detection algorithm, especially when the

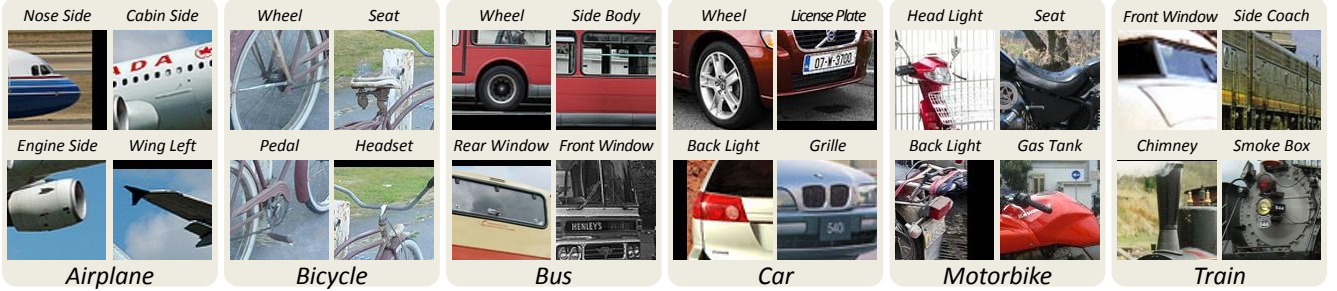


Figure 1: Typical semantic parts from the VehicleSemanticPart dataset (Wang et al. 2015a).

occlusion level is high. It also produces comparable results when the testing images are occlusion-free, and enjoys much lower model complexity (the number of parameters of Deep-Voting is one order of magnitude lower than that of Faster-RCNN, and the average testing speed is $2.5\times$ faster). In diagnosis, we verify that our novel detection framework indeed leads to the advantage over Faster-RCNN. Moreover, it provides the possibility to explain the detection results via looking up the voted visual concepts.

Related Work

Deep convolutional neural networks have been applied to a wide range of computer vision problems, including image recognition (Krizhevsky, Sutskever, and Hinton 2012; Simonyan and Zisserman 2015; Szegedy et al. 2015; He et al. 2016; Huang et al. 2017), semantic segmentation (Long, Shelhamer, and Darrell 2015; Chen et al. 2017; Zheng et al. 2015), object detection (Girshick et al. 2014; Girshick 2015; Ren et al. 2015; Lin et al. 2017; He et al. 2017), etc. These object detection approaches are based on one type of flowchart, which first extracts a number of regions named object proposals (Alexe, Deselaers, and Ferrari 2012; Uijlings et al. 2013), then determines if each of them belongs to the target class, with bounding box regression applied. Non-maximum suppression is attached as a post-processing method to obtain final detection results. This framework significantly outperforms the deformable part-based model (Felzenszwalb et al. 2010) trained on top of a set of handcrafted features (Dalal and Triggs 2005).

Finding object parts is an important problem beyond object detection. The detected parts can directly assist object detection (Felzenszwalb et al. 2010; Zhu, Chen, and Yuille 2015), be used for a fine-scaled description of the object (Zhang et al. 2014), or serve as auxiliary cues to understand classification (Huang et al. 2016), object detection or segmentation (Wang et al. 2015b). Part detection is especially difficult when the object is partially missing and/or occluded. In this scenario, either a flexible model is applied to allow the absence of some components (Chen et al. 2014), or the hidden parts need to be inferred based on the spatial or geometric cues of other parts (Chen and Yuille 2015).

In this paper, we consider mid-level representation of deep networks named *visual concepts* (Wang et al. 2015a), and design a bottom-up voting mechanism to integrate these

weak visual cues for semantic part detection. Geometric constraints (Felzenszwalb et al. 2010) are incorporated via learning a spatial heatmap, *i.e.*, the spatial distribution of the visual cues related to the detection target (Dai et al. 2016). We propose to train our network using occlusion-free images, as we do not need to generate a very large training set to cover as many occlusion patterns as possible.

The DeepVoting Framework

Motivation

We aim at detecting the semantic parts of an object under occlusion. Some representative semantic parts are shown in Figure 1. First of all, we argue that occlusion-free images should be used in the training phase, because the appearance and position of the occluders can be arbitrary, and it is almost impossible to cover all of them by a limited training set. It is our goal to design a framework which can transfer from the occlusion-free domain to the occlusion domain.

One possible solution is to adapt the state-of-the-art object detection methods, such as Faster-RCNN (Ren et al. 2015). These methods first extract a number of proposals for semantic parts and then compute the classification scores for each of them. But, we point out that this strategy may miss some partially or fully occluded parts because of two important factors. First, occlusion largely distracts the proposal network from extracting reasonable objectness regions. Second, the appearance of the occluded parts can be totally different, so that the classification stage also suffers. We verify that these factors indeed downgrade the performance of Faster-RCNN in Table 1.

To deal with these problems, we propose an alternative strategy, which accumulates mid-level visual cues to detect high-level semantic parts. We define these mid-level cues to be *visual concepts* (Wang et al. 2015a), *i.e.*, a set of intermediate CNN states which are closely related to semantic parts. A semantic part is supported by several visual concepts. Even if some of them are missing due to occlusion, it is possible to infer the presence of the semantic part via the remaining ones.

Note that the visual concepts are extracted when the objects appear at a fixed scale (Wang et al. 2015a), since each neuron on the *pool-4* layer has a fixed receptive field size (Simonyan and Zisserman 2015). Therefore, **we assume that**

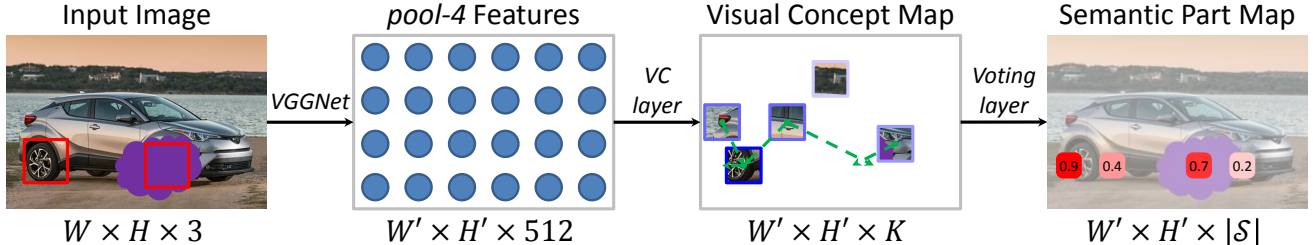


Figure 2: The overall framework of DeepVoting (best viewed in color). A car image with two wheels (marked by red frames, one of them is occluded) is fed into VGGNet, and the intermediate outputs are passed through a visual concept extraction layer and a voting layer. We aggregate local cues from the visual concept map (darker blue indicates more significant cues), consider their spatial relationship to the target semantic part via voting, and obtain a low-resolution map of semantic parts (darker red or a larger number indicates higher confidence). Based on this map, we perform bounding box regression followed by non-maximum suppression to obtain the final results.

the object scale is approximately the same in both training and testing stages. We achieve this at the testing stage via a standalone network for scale prediction.

Formulation

Let an image \mathbf{I} be a $W \times H$ matrix with RGB channels at each pixel. This image is fed into a 16-layer VGGNet (Simonyan and Zisserman 2015), and we follow (Wang et al. 2015a) to consider the *pool-4* features as a set of intermediate neural responses, since these activity values contain some mid-level visual representations which are directly related to semantic part detection. Denote the output of the *pool-4* layer as \mathbf{X} , or a $W' \times H' \times D$ cube, where W' and H' are the down-sampled scales of W and H , and $D = 512$ according to the configuration of VGGNet. These responses can be considered as $W' \times H'$ high-dimensional vectors, and each of them represents the appearance of a local region. Denote each D -dimensional neural response vector as \mathbf{x}_i where i is an index at the $W' \times H'$ grid. These vectors are ℓ_2 -normalized so that the magnitude of each feature is the same.

Visual Concept Extraction In (Wang et al. 2015a), a set of visual concepts $\mathcal{V} = \{\mathbf{v}_1, \dots, \mathbf{v}_K\}$ are extracted, and each visual concept is considered intuitively as a repeatable template to capture the mid-level semantics from these neural responses. It applies K -Means clustering to obtain these visual concepts, and the relationship between each pair of visual concept \mathbf{v}_k and *pool-4* vector \mathbf{x}_i is measured by the ℓ_2 -distance, *i.e.*, $\|\mathbf{v}_k - \mathbf{x}_i\|_2^2$. We note that $\|\mathbf{x}_i\|_2 = 1$ has unit length and $\|\mathbf{v}_k\|_2 \approx 1$ as it is averaged over a set of neighboring \mathbf{x}_i 's, so we have $\|\mathbf{v}_k - \mathbf{x}_i\|_2^2 \approx 2 - 2 \langle \mathbf{v}_k, \mathbf{x}_i \rangle$ where $\langle \cdot, \cdot \rangle$ is the inner-product of two vectors. This motivates us to implement this module as a convolutional layer and plug it into the deep learning framework.

The kernel size of this convolutional layer is set to be 1×1 , *i.e.*, each \mathbf{x}_i is considered individually. The ReLU activation (Nair and Hinton 2010) follows to set the negative responses as 0's and thus avoids them from providing negative cues. This is driven by the requirement of dealing with occlusion, *i.e.*, the presence of a visual concept can pro-

vide positive cues for the existence of a part, but the absence of a visual concept shall not provide the opposite information, since this may be caused by occlusion. We append a dropout layer (Srivastava et al. 2014) with a drop ratio 0.5, so that a random subset of the visual concepts are discarded in the training process. This strategy facilitates the model to perform detection using incomplete information and, consequently, improves the testing accuracy when occlusion is present.

The output of visual concept extraction is a map \mathbf{Y} of size $W' \times H' \times |\mathcal{V}|$, where \mathcal{V} is the set of visual concepts. We set $|\mathcal{V}| = 256$, though a larger set may lead to slightly better performance. Although these visual concepts are trained from scratch rather than obtained from clustering (Wang et al. 2015a), we will show in Figure 4 that they are also capable of capturing repeatable visual patterns.

Semantic Part Detection via the Voting Layer After the previous stage, we can find some *fired* visual concepts, *i.e.*, those positions with positive response values. We accumulate them for part detection by considering the spatial relationship between each pair of visual concept and semantic part. It is motivated by the nature that a visual concept can, at least weakly, suggest the existence of a semantic part. For example, as shown in Figure 2, in a car image, finding a *headlight* implies that there is a *wheel* nearby, and the distance and direction from the *headlight* to the *wheel* are approximately the same under a fixed scale.

These cues are aggregated with another convolutional layer, named the voting layer, in which we set the receptive field of each convolutional kernel to be large, *e.g.*, 15×15 , so that a visual concept can vote for the presence of a semantic part at a relatively long distance. This strategy helps especially when the object is partially occluded, as effective visual cues often emerge outside the occluder and may be far from the target (see Figure 6 for qualitative verifications). Each convolutional kernel in this layer is referred to as a spatial *heatmap*, since it represents the frequency that a visual concept appears at different relative positions. Some heatmaps are visualized in Figure 4.

Denote the output of the voting layer, *i.e.*, the semantic

part map, as \mathbf{Z} . It is a $W' \times H' \times |\mathcal{S}|$ cube where \mathcal{S} is the set of semantic parts. Each local maximum at the semantic part map corresponds to a keypoint on the image lattice. To generate a bounding box for part detection, we set an anchor box, sized 100×100 and centered at the keypoint, and learn the spatial rescaling and translation to regress the anchor box (Girshick et al. 2014) based on the training data. The basic size 100×100 is the average semantic part scale over the entire training dataset (Wang et al. 2015a).

Training and Testing

We train the network on an occlusion-free image corpus. This helps us obtain clear relationship between each pair of visual concept and semantic part. We also discard the background region by cropping the object according to the ground-truth bounding box, so as to maximally alleviate the impact brought by the background clutters. Then, we rescale the image so that the short edge contains 224 pixels, which is motivated by (Wang et al. 2015a) to capture the visual concepts at a fixed scale. The image is fed into the 16-layer VGGNet, and we obtain the feature vectors at the *pool-4* layer.

These feature vectors are normalized and passed through two layers for visual concept extraction and voting. We compare the semantic part map \mathbf{Z} with the ground-truth annotation \mathbf{L} by computing dice coefficient between prediction and ground-truth (Milletari, Navab, and Ahmadi 2016). For this, we find four nearest grid points at the $W' \times H'$ grid (down-sampled from the original image by the factor of 16) based on the center pixel of each annotated semantic part, and set the labels of these positions as 1 and others as 0. The label cube \mathbf{L} is also of size $W' \times H' \times |\mathcal{S}|$. The similarity between \mathbf{Z} and \mathbf{L} is defined as:

$$\mathcal{D}(\mathbf{Z}, \mathbf{L}) = \frac{1}{|\mathcal{S}|} \sum_{s=1}^{|\mathcal{S}|} \frac{2 \times \sum_{w=1, h=1}^{W', H'} z_{w, h, s} \times l_{w, h, s}}{\sum_{w=1, h=1}^{W', H'} (z_{w, h, s}^2 + l_{w, h, s}^2)}, \quad (1)$$

It is straightforward to compute the gradients based on the loss function $\mathcal{L}(\mathbf{Z}, \mathbf{L}) = 1 - \mathcal{D}(\mathbf{Z}, \mathbf{L})$.

On the testing stage, we first use ScaleNet (see the next subsection) to obtain the object scale. Then, we rescale the image so that the short edge of the object box approximately contains 224 pixels. We do not crop the object because we do not know its exact location. Then, the image is passed through the VGGNet followed by both visual concept extraction and voting layers, and finally we apply the spatial rescaling and translation to the anchor box (100×100) towards more accurate localization. A standard non-maximum suppression is performed to finalize the detection results.

The Scale Prediction Network

The above framework is based on an important assumption, that an object always appears in approximately the same scale. This is due to two reasons. First, as shown in (Wang et al. 2015a), the visual concepts emerge when the object is rescaled to the same scale, *i.e.*, the short edge of the object bounding box contains 224 pixels. Second, we expect the voting layer to learn fixed spatial offsets which relate a visual concept to a semantic part. As an example, the heatmap

delivers the knowledge that in the side view of a *car*, the *headlight* often appears at the upperleft direction of a *wheel*, and the spatial offset on x and y axes are about 64 and 48 pixels (4 and 3 at the *pool-4* grid), respectively. Such information is not scale-invariant.

To deal with these issues, we introduce an individual network, namely the ScaleNet (Qiao et al. 2017), to predict the object scale in each image. The main idea is to feed an input image to a 16-layer VGGNet for a regression task (the *fc-8* layer is replaced by a 1-dimensional output), and the label is the ground-truth object size. Each input image is rescaled, so that the long edge contains 224 pixels. It is placed at the center of a 224×224 square and the remaining pixels are filled up with the averaged intensity. In the training stage, we consider the short edge of the object, and ask the deep network to predict the ratio of the object short edge to the image long edge (224 pixels). In the testing stage, an image is prepared and fed into the network in the same flowchart, and the predicted ratio is used to normalize the object to the desired size, *i.e.*, its short edge contains 224 pixels.

Discussions and Relationship to Previous Work

The overall framework of DeepVoting is quite different from the conventional proposal-based detection methods, such as Faster-RCNN (Ren et al. 2015) and R-FCN (Dai et al. 2016). This is mainly due to the problem setting, *i.e.*, when the occlusion is present, the accuracy of both proposal and classification networks becomes lower. However, DeepVoting is able to infer the occluded parts via accumulating those non-occluded visual cues. We will show more comparative experiments in the experiment section.

We decompose semantic part detection into two steps, *i.e.*, central pixel detection and bounding box regression. The first step is performed like semantic segmentation (Long, Shelhamer, and Darrell 2015) in a very low-resolution setting (down-sampled from the original image by the factor of 16). This is a novel idea for detection. We also borrow the idea from segmentation (Milletari, Navab, and Ahmadi 2016), which uses a loss function related to the dice coefficient in optimization. As the semantic part is often much smaller compared to the entire image, this strategy alleviates the bias of data imbalance, *i.e.*, the model is more likely to predict each pixel as background as it appears dominantly in the training data.

All the network modules can be set more complicated to achieve better detection accuracy, *e.g.*, we can apply a stronger backbone for intermediate feature extraction (we believe the performance would be better). We can also stack multiple layers for visual concept extraction and/or voting, but we avoid this in order to make our detection results easier to explain. In practice, this structure is strong enough to beat the state-of-the-art object detection methods under occlusion.

Experiments

Dataset and Baseline

We use the **VehicleSemanticPart** dataset (Wang et al. 2015a) for semantic part detection. This dataset contains



Figure 3: Examples of images with occlusion. The first is the original occlusion-free image. For the second, third and forth image (in row-major order), there are 2, 3 and 4 occluders, and the occluded ratio of object, computed by pixels, is 0.2–0.4, 0.4–0.6 and 0.6–0.8, respectively.

4549 training images and 4507 testing images covering six types of vehicles, *i.e.*, *airplane*, *bicycle*, *bus*, *car*, *motorbike* and *train*. In total, 133 semantic parts are annotated. Some typical semantic parts are displayed in Figure 1.

Since there is no public occlusion dataset with semantic parts labelled, and it would be extremely difficult and expensive to label the semantic parts which are truly occluded, we follow the similar procedure in (Li and Malik 2016) to synthesize an occlusion dataset. For each test image in **Vehicle-SemanticPart** dataset, we place some randomly-positioned occluders (irrelevant to the target object) and make sure that the occlusion ratio of the target object is constrained.

We train six models, one for each object class. All the models are trained on an occlusion-free dataset (the motivation is elaborated in the previous sections), but evaluated on either non-occluded images, or the images with different levels of occlusions added. In the latter case, we vary the difficulty level by occluding different fractions of the object. We evaluate all the competitors following a popular criterion (Everingham et al. 2010), which computes the mean average precision (mAP) based on the list of detected parts. A detected box is considered to be true-positive if and only if its IoU rate with a ground-truth box is not lower than 0.5. Each semantic part is evaluated individually, and the mAP of each object class is the average mAP over all the semantic parts.

DeepVoting (denoted as **DV**) is compared with two baselines. The first one is to directly use visual concepts to detect the semantic parts. These visual concepts can be extracted by two different methods, *i.e.*, either clustered from a set of *pool-4* features (using *K*-Means as in (Wang et al. 2015a), denoted as **KVC**), or directly obtained from DeepVoting (the weights of the visual concept extraction layer, denoted as **DVC**). In both cases, we use the ScaleNet as in DeepVoting. The second one is Faster-RCNN (Ren et al. 2015) (denoted as **FR**), the state-of-the-art algorithm for object detection, which is also capable of part detection. Here, **we train models for each category, and each semantic part of a category is considered as a separate class for training**, *i.e.*, on each category, we train a model with $|\mathcal{S}| + 1$ classes, corresponding to $|\mathcal{S}|$ semantic parts and the background.

Semantic Part Detection without Occlusion

As a simplified task, we evaluate our algorithm in detecting semantic parts on non-occluded objects. This is also a baseline for later comparison. In the left four columns of Ta-

ble 1, we list the detection accuracy produced by different methods. The average detection accuracy by DeepVoting is significantly higher than using single visual concepts for detection, regardless whether the visual concepts are obtained from *K*-Means clustering or DeepVoting. This shows the advantage of our approach which aggregates multiple visual cues for detection, meanwhile allowing joint optimization of both weights for visual concept extraction and voting.

On the other hand, DeepVoting produces slightly lower detection accuracy compared to Faster-RCNN. We argue that Faster-RCNN benefits from the proposal network which generates high quality proposals and the deeper multilayer fully-connected classifier, but this mechanism is less robust under occlusion. In particular, with 10 \times more parameters, Faster-RCNN may be easily over-fitted to the training dataset which is occlusion-free. Consequently, it performs well on the occlusion-free testing images, but is vulnerable to occlusions. Meanwhile, DeepVoting enjoys lower computational overheads, *i.e.*, it runs 2.5 \times faster in testing.

Visualizing Visual Concepts and Spatial Heatmaps In Figure 4, we show some typical examples of the learned visual concepts and spatial heatmaps. The visualization of visual concepts follows the approach used in (Wang et al. 2015a), which finds 10 most significant responses on each convolutional filter, *i.e.*, the matching template, traces back to the original image lattice, and crops the region corresponding to the neuron at the *pool-4* layer. To show different spatial heatmaps, we randomly choose some relevant pairs of visual concept and semantic part, and plot the convolutional weights of the voting layer for comparison.

Scale Prediction Accuracy We investigate the accuracy of ScaleNet, which is essential for scale normalization. For each testing image, we compute the ratio of the predicted object scale to the actual scale, and plot the contribution of this ratio over the entire testing set in Figure 5. One can see that in more than 75% cases, the relative error of the predicted scale does not exceed 10%. Actually, these prediction results are accurate enough for DeepVoting. Even provided with the oracle scale, the mean detection accuracy over six objects is slightly improved from 70.6% to 72.5%.

Semantic Part Detection under Occlusion

We further detect semantic parts when the object is occluded in three different levels. In the first level (denoted

Category	No Occlusions				L1			L2			L3		
	KVC	DVC	FR	DV	FR	DV	Gain	FR	DV	Gain	FR	DV	Gain
airplane	15.8	26.6	56.9	57.2	35.4	38.7	+9.3	27.0	29.8	+10.5	20.1	23.9	+19.1
bicycle	58.0	52.3	90.6	88.2	77.0	81.9	+6.4	62.0	76.7	+23.7	41.1	61.2	+48.9
bus	23.8	25.1	86.3	75.8	55.5	53.7	-3.4	40.1	41.4	+3.2	25.8	28.5	+10.5
car	25.2	36.5	83.9	78.2	48.8	52.4	+7.5	30.9	35.8	+15.9	19.8	23.4	+18.0
motorbike	32.7	29.2	63.7	63.4	42.2	50.0	+18.6	32.4	39.9	+23.1	20.1	28.4	+41.4
train	12.3	12.8	59.9	60.7	30.6	33.6	+9.6	17.7	19.3	+9.0	10.9	13.9	+27.3
mean	28.0	30.4	73.6	70.6	48.3	51.7	+7.2	35.0	40.5	+15.6	23.0	29.9	+30.2

Table 1: Left 4 columns: Comparison of detection accuracy (mean AP, %) without occlusion. Right 9 columns: Comparison of detection accuracy (mean AP, %) when the object is occluded by three different levels. We do not show KVC or DVC numbers as they are much lower than FR and DV ones. The final column of each part is the *relative gain* (%) of DV over FR. See the texts for details.

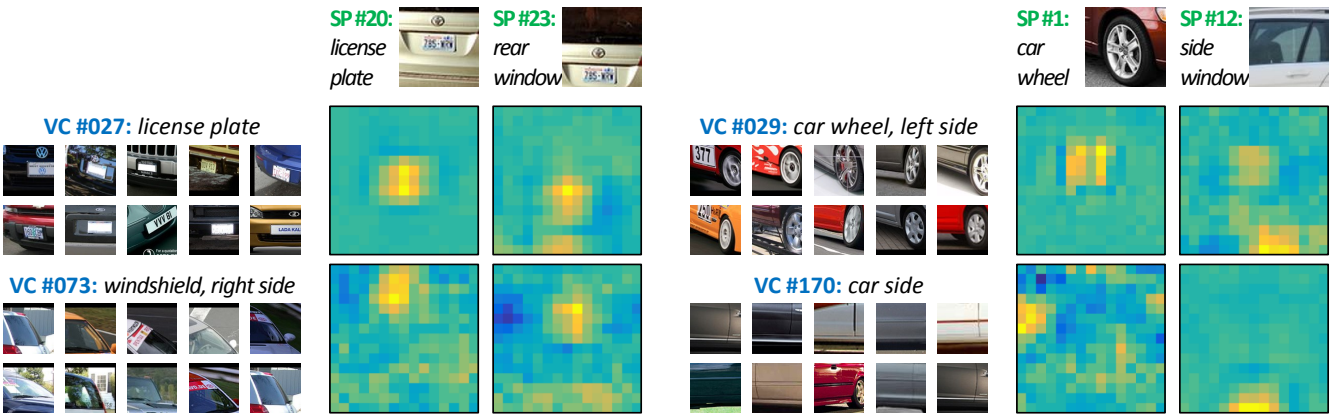


Figure 4: Visualization of visual concepts and spatial heatmaps (best viewed in color). For each visual concept, we show 10 patches with the highest responses. Each spatial heatmap illustrates the cues to detect a semantic part, in which yellow, cyan and dark blue indicate positive, zero and negative cues, respectively. For example, VC #073 (*windshield*) often appears above SP #20 (*license plate*), and VC #170 (*car side bottom*) often appears below SP #12 (*side window*).

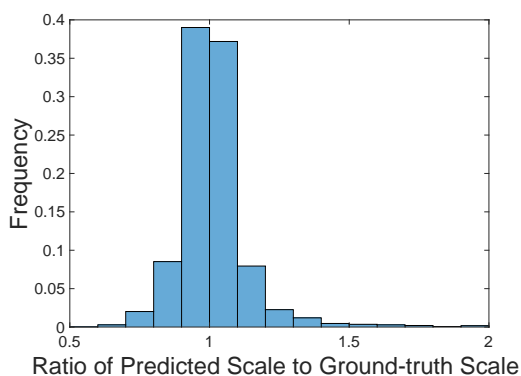


Figure 5: The distribution of the ratio of the predicted scale to the actual scale.

as **L1**), we place 2 occluders on each object, and the occluded ratio r of the object, computed by pixels, satisfying $0.2 \leq r < 0.4$. For **L2** and **L3**, we have 3 and 4 occluders, and $0.4 \leq r < 0.6$ and $0.6 \leq r < 0.8$, respectively

(see Figure 3 for examples). For convenience, the original occlusion-free testing set is denoted as **L0**. The detection results are summarized in Table 1. One can see that Deep-Voting outperforms the Faster-RCNN significantly in these cases, and especially, the accuracy gain increases as the occlusion level goes up, suggesting the advantage of DeepVoting in detecting occluded semantic parts.

As a side evidence, we investigate the impact of the size of spatial heatmap (the kernel of the voting layer). At the heaviest occlusion level, when we shrink the default 15×15 to 11×11 , the mean detection accuracy drops from 29.9% to 28.5%, suggesting the usefulness of long-distance voting in detecting occluded parts. When the kernel size is increased to 19×19 , the accuracy is slightly improved to 30.5%. We keep it as 15×15 for lower model complexity.

To verify our motivation that Faster-RCNN suffers downgraded performance in both the proposal network and the classifier, we investigate both the recall of the proposals and the accuracy of the classifier. Results are summarized in Table 2. First, we can see that the recall of the proposals goes down significantly as the occlusion level goes up, since the objectness of the semantic part region may become

Category	Recall at Different Levels				mAP w/ Addt'l Prop.			mAP by DeepVoting		
	L0	L1	L2	L3	L1	L2	L3	L1	L2	L3
airplane	99.3	98.1	97.4	96.7	36.2	27.7	20.7	38.7	29.8	23.9
bicycle	99.5	99.0	98.0	96.5	77.9	64.0	44.7	81.9	76.7	61.2
bus	99.8	96.3	93.8	91.5	57.1	42.4	28.3	53.7	41.4	28.5
car	99.8	96.0	94.4	92.7	48.2	30.2	19.4	52.4	35.8	23.4
motorbike	99.0	96.5	95.7	93.3	43.6	33.1	21.3	50.0	39.9	28.4
train	98.3	93.5	90.6	85.6	32.0	19.4	11.3	33.6	19.3	13.9
mean	99.3	96.6	95.0	92.7	49.2	36.1	24.2	51.7	40.5	29.9

Table 2: Left 4 columns: the recall rates produced by the proposal network at different occlusion levels. Middle 3 columns and right 3 columns: the comparison of Faster-RCNN (equipped with additional proposals from ground-truth bounding boxes) and DeepVoting detection results.

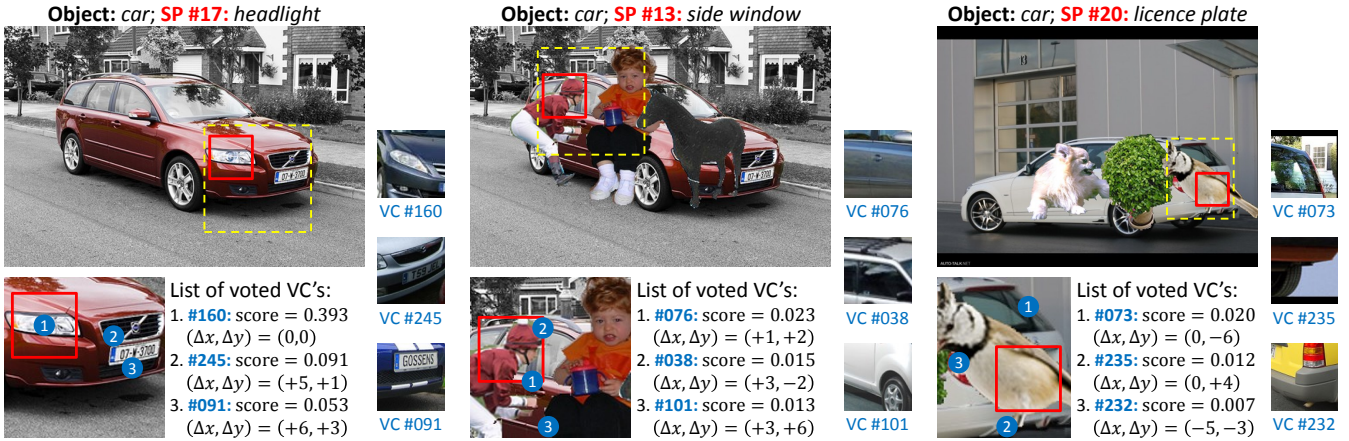


Figure 6: DeepVoting allows us to explain the detection results. In the example of heavy occlusion (the third column), the target semantic part, *i.e.*, the *licence plate* on a *car*, is fully occluded by a *bird*. With the help of some visual concepts (blue dots), especially the 73-rd VC (also displayed in Figure 4), we can infer the position of the occluded part (marked in red). Note that we only plot the 3 VC's with the highest scores, regardless the number of voting VC's can be much larger.

weaker due to the randomly placed occluders. Thus the second stage, *i.e.*, classification, has to start with a relatively low-quality set of candidates. In the second part, we add the ground-truth bounding boxes to the existing proposals so that the recall is 100%, feed these candidates to the classifier, and evaluate its performance on the occluded images. Even with such benefits, Faster-RCNN still produces unsatisfying detection accuracy. For example, in detecting the semantic parts of a *bicycle* at the highest occlusion level (**L3**), making use of the additional proposals from ground-truth bounding boxes merely improves the detection accuracy from 41.1% to 44.7%, which is still much lower than the number 61.2% produced by DeepVoting. This implies that the classifier may be confused since the occluder changes the appearance of the proposals.

Explaining the Detection Results

Finally, we show an intriguing benefit of our approach, which allows us to explain the detection results. In Figure 6, we display three examples, in which the target semantic parts are not occluded, partially occluded and fully occluded, respectively. DeepVoting is not only able to infer

the occluded semantic parts, but also capable of looking up the voting visual concepts for diagnosis. This allows us to dig into errors and understand the working mechanism of our approach.

Conclusions

In this paper, we propose a novel framework named **Deep-Voting** for semantic part detection under occlusion. The intermediate visual representations named *visual concepts* are extracted and used to vote for semantic parts via two convolutional layers. The spatial relationship between visual concepts and semantic parts is learned from a occlusion-free dataset and then transferred to the occluded testing images. DeepVoting is evaluated on the **VehicleSemanticPart** dataset, and shows superior performance to Faster-RCNN, the state-of-the-art detection method, in the occlusion scenario. Our approach also enjoys the advantage of being explainable, which allows us to diagnose the semantic parts detection results via checking the contribution of each voting visual concepts.

References

Alexe, B.; Deselaers, T.; and Ferrari, V. 2012. Measuring the objectness of image windows. *IEEE Transactions on Pattern Analysis and Machine Intelligence* 34(11):2189–2202.

Chen, X., and Yuille, A. L. 2015. Parsing occluded people by flexible compositions. In *Computer Vision and Pattern Recognition*. IEEE.

Chen, X.; Mottaghi, R.; Liu, X.; Fidler, S.; Urtasun, R.; and Yuille, A. 2014. Detect what you can: Detecting and representing objects using holistic models and body parts. In *Computer Vision and Pattern Recognition*. IEEE.

Chen, L.-C.; Papandreou, G.; Kokkinos, I.; Murphy, K.; and Yuille, A. L. 2017. Deeplab: Semantic image segmentation with deep convolutional nets, atrous convolution, and fully connected crfs. *IEEE Transactions on Pattern Analysis and Machine Intelligence*.

Dai, J.; Li, Y.; He, K.; and Sun, J. 2016. R-fcn: Object detection via region-based fully convolutional networks. In *Advances in Neural Information Processing Systems*.

Dalal, N., and Triggs, B. 2005. Histograms of oriented gradients for human detection. In *Computer Vision and Pattern Recognition*. IEEE.

Everingham, M.; Van Gool, L.; Williams, C. K.; Winn, J.; and Zisserman, A. 2010. The pascal visual object classes (voc) challenge. *International Journal of Computer Vision* 88(2):303–338.

Felzenszwalb, P. F.; Girshick, R. B.; McAllester, D.; and Ramanan, D. 2010. Object detection with discriminatively trained part-based models. *IEEE Transactions on Pattern Analysis and Machine Intelligence* 32(9):1627–1645.

Girshick, R.; Donahue, J.; Darrell, T.; and Malik, J. 2014. Rich feature hierarchies for accurate object detection and semantic segmentation. In *Computer Vision and Pattern Recognition*. IEEE.

Girshick, R. 2015. Fast r-cnn. In *International Conference on Computer Vision*. IEEE.

He, K.; Zhang, X.; Ren, S.; and Sun, J. 2016. Deep residual learning for image recognition. In *Computer Vision and Pattern Recognition*. IEEE.

He, K.; Gkioxari, G.; Dollár, P.; and Girshick, R. 2017. Mask r-cnn. *arXiv preprint arXiv:1703.06870*.

Huang, S.; Xu, Z.; Tao, D.; and Zhang, Y. 2016. Part-stacked cnn for fine-grained visual categorization. In *Computer Vision and Pattern Recognition*. IEEE.

Huang, G.; Liu, Z.; van der Maaten, L.; and Weinberger, K. Q. 2017. Densely connected convolutional networks. In *Computer Vision and Pattern Recognition*. IEEE.

Krizhevsky, A.; Sutskever, I.; and Hinton, G. E. 2012. Imagenet classification with deep convolutional neural networks. In *Advances in Neural Information Processing Systems*.

Li, K., and Malik, J. 2016. Amodal instance segmentation. In *European Conference on Computer Vision*. Springer.

Lin, T.-Y.; Dollár, P.; Girshick, R.; He, K.; Hariharan, B.; and Belongie, S. 2017. Feature pyramid networks for object detection. In *Computer Vision and Pattern Recognition*. IEEE.

Long, J.; Shelhamer, E.; and Darrell, T. 2015. Fully convolutional networks for semantic segmentation. In *Computer Vision and Pattern Recognition*. IEEE.

Milletari, F.; Navab, N.; and Ahmadi, S.-A. 2016. V-net: Fully convolutional neural networks for volumetric medical image segmentation. In *International Conference on 3D Vision*. IEEE.

Nair, V., and Hinton, G. E. 2010. Rectified linear units improve restricted boltzmann machines. In *International Conference on Machine Learning*.

Qiao, S.; Shen, W.; Qiu, W.; Liu, C.; and Yuille, A. 2017. Scalenet: Guiding object proposal generation in supermarkets and beyond. *arXiv preprint arXiv:1704.06752*.

Ren, S.; He, K.; Girshick, R.; and Sun, J. 2015. Faster r-cnn: Towards real-time object detection with region proposal networks. In *Advances in Neural Information Processing Systems*.

Simonyan, K., and Zisserman, A. 2015. Very deep convolutional networks for large-scale image recognition. In *International Conference on Learning Representations*.

Srivastava, N.; Hinton, G. E.; Krizhevsky, A.; Sutskever, I.; and Salakhutdinov, R. 2014. Dropout: a simple way to prevent neural networks from overfitting. *Journal of Machine Learning Research* 15(1):1929–1958.

Szegedy, C.; Liu, W.; Jia, Y.; Sermanet, P.; Reed, S.; Anguelov, D.; Erhan, D.; Vanhoucke, V.; and Rabinovich, A. 2015. Going deeper with convolutions. In *Computer Vision and Pattern Recognition*. IEEE.

Uijlings, J. R.; Van De Sande, K. E.; Gevers, T.; and Smeulders, A. W. 2013. Selective search for object recognition. *International Journal of Computer Vision* 104(2):154–171.

Wang, J.; Zhang, Z.; Xie, C.; Premachandran, V.; and Yuille, A. 2015a. Unsupervised learning of object semantic parts from internal states of cnns by population encoding. *arXiv preprint arXiv:1511.06855*.

Wang, P.; Shen, X.; Lin, Z.; Cohen, S.; Price, B.; and Yuille, A. L. 2015b. Joint object and part segmentation using deep learned potentials. In *International Conference on Computer Vision*. IEEE.

Zhang, N.; Donahue, J.; Girshick, R.; and Darrell, T. 2014. Part-based r-cnns for fine-grained category detection. In *European Conference on Computer Vision*. Springer.

Zheng, S.; Jayasumana, S.; Romera-Paredes, B.; Vineet, V.; Su, Z.; Du, D.; Huang, C.; and Torr, P. H. 2015. Conditional random fields as recurrent neural networks. In *International Conference on Computer Vision*. IEEE.

Zhu, J.; Chen, X.; and Yuille, A. L. 2015. Deepm: A deep part-based model for object detection and semantic part localization. *arXiv preprint arXiv:1511.07131*.